Proceedings World Geothermal Congress 2005
Antalya, Turkey, 24-29 April 2005

Steam-Water Capillary Pressure

Kewen Li and Roland N. Horne

Stanford Geothermal Program, Stanford University, Stanford, CA 94305-2220, USA

kewenli@stanford.edu and horne@stanford.edu

Keywords:steam-water, capillary pressure, model, fractal

ABSTRACT

Steam-water capillary pressure is of central importance in geothermal reservoir engineering, however it is still poorly known due to the difficulty making direct measurements. To this end, we have conducted experimental and theoretical studies over the past five years and have made significant progress in understanding fundamental steam-water flow. In this paper, we summarize and discuss the results.

Methods to measure steam-water and air-water capillary pressures were developed using an X-ray CT scanner. Both steam-water and air-water capillary pressures were measured and compared. It was found that there are significant differences between steam-water and air-water capillary pressures. So we may not substitute air-water capillary pressure data in steam-water flow calculations. Using data measured from steady-state steam-water flow, an empirical model was developed to calculate steam-water capillary pressure directly. The only required reservoir parameters are porosity, permeability, and temperature.

Also developed was a generalized capillary pressure model from fractal modeling of a porous medium. The model encompasses the frequently used Brooks-Corey model and the Li-Horne model. This also demonstrates that the two models, both of which have been considered as empirical, have a solid theoretical basis. We also showed that steam-water relative permeability could be calculated from capillary pressure based on a generalized relative permeability model, which is derived from the generalized capillary pressure model.

1. INTRODUCTION

Steam-water capillary pressure is often either ignored or considered in an approximate way in numerical simulations or other calculations in geothermal reservoir engineering. However steam-water capillary pressure plays an important role in geothermal reservoirs in controlling fluid distribution, transfer of liquid between fractures and matrix, well productivity, and even the reserves.

For example, Tsypkin and Calore (1999) developed a mathematical model of steam-water phase transitions. They found that steam-water capillary pressure could play a stabilizing role for the vaporization front, causing a sharp zone to develop. Urmeneta *et al*. (1998) also studied the role of capillary forces in fractured reservoirs and found that capillary pressure tended to keep the vapor phase in the fracture and the liquid phase in the matrix.

Using the adsorption data of Horne *et al*. (1995) for rock samples from The Geysers geothermal field, Sta. Maria and Pingol (1996) inferred the values of steam-water capillary pressure. They found the steam-water capillary pressure to range from 0 to 5,850 atm. Persoff and Hulen (1996) also inferred the capillary pressure from adsorption data of The Geysers rock samples and found the steam-water capillary pressure ranging from 0 to about 1,905 atm. The graywacke core samples used by Persoff and Hulen (1996) were similar to those used by Sta. Maria and Pingol (1996). The porosity was about 2% and the permeability in the nanodarcy (nd) range.

There are two main methods to measure steam-water capillary pressure. One is the adsorption/desorption (Horne et al., 1995; Sta. Maria and Pingol, 1996) and another is the fluid flow approach (Li and Horne, 2001). The adsorption/desorption tests that have been used to infer steam-water capillary pressure are static processes in which there is no steam-water flow. In actual geothermal reservoirs, however, capillary pressure plays an important role while steam and water flow simultaneously through the rocks. Hence the process governing an adsorption test may not represent the mechanisms under actual fluid flow conditions in those reservoirs. The steam-water capillary pressures from adsorption data may or may not be the same as those measured using a dynamic method in which steam and water are flowing.

Using a fluid flow approach, it is difficult to measure steam-water capillary pressure due to the phase transformation and the significant mass transfer between the two phases as pressure changes.

There has been some discussion regarding the differences between steam-water and air-water flow through a porous medium in recent years. If there are no differences between the two, we could represent steam-water flow by air-water flow in which capillary pressure can be measured easily. Sanchez and Schechter (1990) reported that the differences between steam-water and nitrogen-water relative permeabilities were almost negligible in an unconsolidated core sample. However, Horne *et al*. (2000) found significant differences in experiments using Berea sandstone with a much lower permeability than that of the core sample used by Sanchez and Schechter (1990). Accordingly, there may also be significant differences between steam-water and nitrogen-water capillary pressures. Unfortunately, few direct comparisons of steam-water and air-water capillary pressures are available due to the scarcity of methods available to measure them.

We investigated capillary pressure in geothermal systems both experimentally and theoretically over the past five years, including steam-water, air-water, and air-mercury capillary pressures. The differences between steam-water and air-water capillary pressure as well as the fundamental mechanisms of steam-water flow in a porous medium were confirmed and understood more through these studies. The results are summarized and discussed in this paper.

2. THEORY

2.1 Computation of Steam-Water Capillary Pressure from Measurement of Vapor Pressure

There were few direct measurements of steam-water capillary pressure before 2000. Li and Horne (2001) derived a formula based on the Kelvin equation, by which steam-water capillary pressure can be calculated using the water phase temperatures and pressures measured by a steady-state flow method. Such a steady-state flow measurement was made by Mahiya (1999). The formula is expressed as follows:

$$p_v - p_w = \frac{\rho_w RT}{M_w} \ln\left(\frac{p_0}{p_v}\right) \quad (1)$$

where p_0 is the vapor pressure when the vapor-liquid interface is flat; p_v is the vapor pressure in a capillary tube of radius r when the vapor-liquid interface is curved; p_w is the pressure of the liquid phase which is the wetting phase in the system studied; R is the gas constant, T the absolute temperature, M_w the molecular weight of liquid, and ρ_w the density of liquid (water in this study).

In the steam-water flow experiments, the pressure (p_w) and temperature (T) of the water phase can be measured at the same time and the same location (Mahiya, 1999), while the saturation pressure on flat surface (p_0) can be calculated according to the measured saturation temperature. Therefore, the vapor pressure (p_v), as the only unknown parameter in Eq. 1, can be obtained using an iterative technique such as the Newton method. The capillary pressure is then computed using the following equation:

$$P_c = p_v - p_w \quad (2)$$

here P_c is the capillary pressure. Eq. 1 was solved iteratively using a spreadsheet in this work.

Note that Eq. 1 is only correct in a capillary tube with a circular shape, based on the derivation. On the other hand, the adsorption process in a porous medium is governed not only by capillary pressure but also by Van der Waals attractive forces, including the dispersion forces. In addition, the electrostatic forces may play an important role. In order to apply Eq. 1 in porous media, we need to assume also that differences of pore shape from circular can be ignored. It may be necessary to make some correction to apply Eq. 1 in a porous medium, in order to meet this assumption as well as all the assumptions inherent in the Kelvin equation itself. In this study, we calculated the vapor pressure using Eq. 1 and then calculated the values of steam-water capillary pressure using Eq. 2.

2.2 Background of the X-Ray CT Technique

An X-ray CT technique has been used in recent years to measure the distribution of steam and water saturation in rocks to obtain steam-water relative permeability curves (Ambusso, 1996; Mahiya, 1999; and Satik, 1998). The steam saturation in a core sample during the measurement of steam-water relative permeability curves is usually calculated using the following equation:

$$S_{st} = \frac{CT_{wet} - CT_{\exp}}{CT_{wet} - CT_{dry}} \quad (3)$$

where S_{st} is the steam saturation; CT_{wet}, CT_{dry} are the CT numbers of the rock when it is fully saturated by water and air respectively; CT_{exp} is the CT number of the rock when it is partially saturated by steam.

The values of CT_{exp} are usually measured at high temperature during the measurements of steam-water flow. The values of CT_{wet} are usually measured at room temperature; CT_{exp} may be less than CT_{wet} even when there is no steam at all in the rock (fully saturated with water). Therefore, the steam saturation calculated using Eq. 3 would be greater than zero, which would not represent the real situation in the rock. To emphasize the effect of temperature on the CT values, Eq. 3 is represented as follows:

$$S_{st} = \frac{CT_{wet}(T) - CT_{\exp}(T)}{CT_{wet}(T) - CT_{dry}(T)} \quad (4)$$

where $CT_{wet}(T)$, $CT_{dry}(T)$ are CT numbers of the rock when it is fully saturated by water and air at a temperature of T, respectively; $CT_{exp}(T)$ is the CT number of the rock when it is partially saturated by steam at the same temperature T.

Once the values of $CT_{wet}(T)$ and $CT_{dry}(T)$ are obtained, porosity can be calculated using the following equation:

$$\phi = \frac{CT_{wet}(T) - CT_{dry}(T)}{CT_{water}(T) - CT_{air}(T)} \quad (5)$$

here CT_{water} and CT_{air} are the CT numbers of water and air at a temperature of T, respectively.

3. EXPERIMENTS

3.1 Imbibition and Drainage Tests

Distilled water was used as the liquid phase; the specific gravity and viscosity were 1.0 and 1.0 cp at 20°C. Steam and air were used as the gas phase; the surface tension of water/air at 20°C was 72.75 dynes/cm. The values of the surface tension at high temperatures were calculated from the ASME Steam Tables. The ceramic sample was provided by Refractron Technologies Corp. and had a porosity of 39.19%, a length of 25.0 cm, an inner diameter of 4.275 cm and an outer diameter of 6.287 cm. We did not measure the permeability of the core sample due to its special shape but the permeability was estimated to be over 10 darcy.

A schematic of the apparatus used to measure both steam-water and air-water capillary pressures in drainage and imbibition is shown in Figure 1.

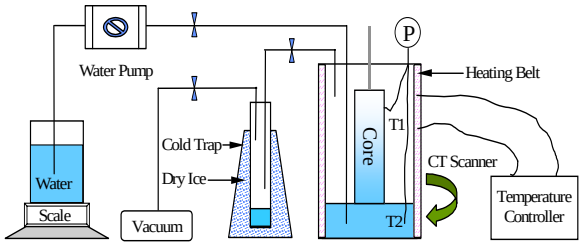

Figure 1: Schematic of the apparatus used to measure both steam-water and air-water capillary pressures.

The core system was assembled in an aluminum cylinder wrapped in a heating belt; the temperature in the cylinder was controlled using an Autotune Temperature Controller (manufactured by OMEGA, Model CN6071A) by turning the heating belt on and off automatically.

The vacuum pump (Welch Technology, Inc., Model 8915) was used to remove the air in the core sample and in the aluminum cylinder in order to generate the steam-water environments.

Water in the aluminum cylinder was delivered by the water pump (Dynamax, Model SD-200, manufactured by RAININ Instrument Co.) and the amount was measured by the scale (Mettler, Model PE 1600) with an accuracy of 0.01g and a range from 0 to 1600g.

3.2 Steady-State Flow Test

The experimental details regarding the collection of the data used to calculate steam-water capillary pressure with Eq. 1 have been presented in the report by Mahiya (1999). For convenience, a brief summary of the steam-water flow tests is given here. Distilled water was used as the liquid phase and to generate steam. A Berea sandstone sample fired at a temperature of 450°C was used; its permeability and porosity were 1400 md and 24.8%; the length and diameter were 43.2 cm and 5.04 cm, respectively.

A schematic of the apparatus is shown in Figure 2 (Mahiya, 1999; Li and Horne, 2001). Automation and data acquisition were realized by using LabView 4.1 and the corresponding hardware (National Instrument Co.).

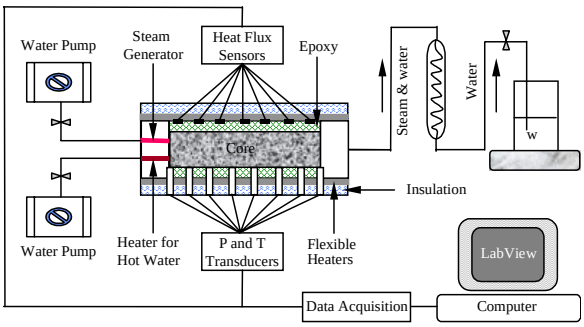

Figure 2: Schematic of steam-water steady-state flow in rock.

3.3 X-ray CT Scanner

The X-ray CT scanner used in this study for measuring the distribution of water saturation along the core was a Picker™ 1200 SX X-ray CT scanner with 1200 fixed detectors. The voxel dimension is 0.5 mm by 0.5 mm by 5 mm, the tube current used in this study was 50 mA, and the energy level of the radiation was 140 keV. The acquisition time of one image is about 3 seconds while the processing time is around 40 seconds.

4. RESULTS

4.1 Differences between Steam-Water and Air-Water Capillary Pressures

4.1.1 Imbibition Case

Using the apparatus shown in Figure 1, Li and Horne (2004a) measured both steam-water and air-water capillary pressures. The results obtained at 98°C are plotted in Figure 3. Air-water capillary pressure was measured at 21°C but scaled to 98°C. Steam-water capillary pressure was measured directly at 98°C. The results demonstrate that steam-water capillary pressure in the ceramic core is about 0.003 atm less than the air-water capillary pressure at the same water saturation in the range from 20 to 85 percent.

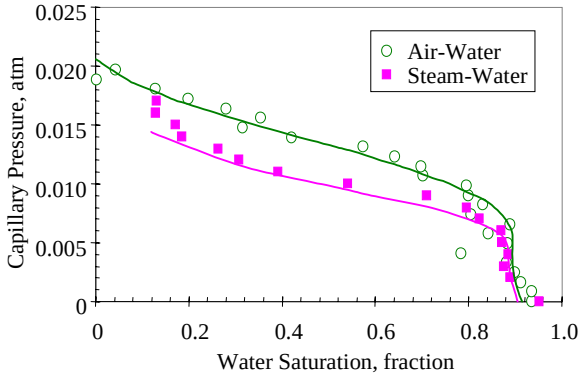

Figure 3: Comparison of imbibition steam-water and air-water capillary pressures at 98°C.

The differences between the steam-water and air-water capillary pressures are significant considering the high permeability of the core sample used. According to the experimental results shown in Figure 3, we would not be able to substitute steam-water capillary pressures simply using air-water capillary pressure measurements. There may be a relationship between the two in which case it may be possible to infer steam-water capillary pressures through air-water capillary pressure measurements. This may be done in the future.

4.1.2 Drainage Case

Li and Horne (2004a) also measured the drainage vapor-water and air-water capillary pressures at 20°C to exclude the possible effect of temperature in the imbibition case (note that the air-water capillary pressures shown in Figure 3 were not measured directly at 98°C). The results obtained from the gravity drainage tests are shown in Figure 4.

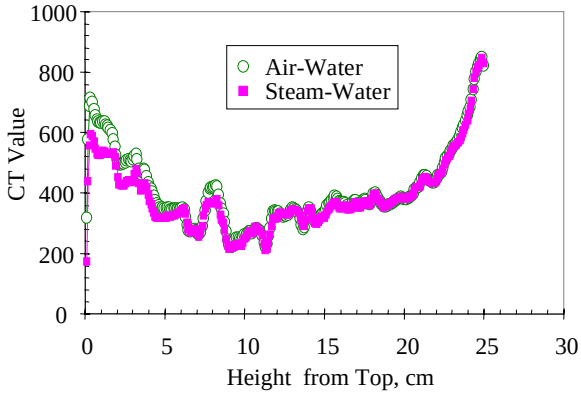

Figure 4: Differences in CT numbers between steam-water and air-water cases after gravity drainage.

The CT number at the same position in the steam-water case is less than that in the air-water case at the top part of the core sample. This implies that the drainage steam-water capillary pressure is less than the drainage air-water capillary pressure at the same water saturation, which is similar to the observation in the imbibition case (see Figure 3). Note that there are almost no differences in CT numbers between steam-water and air-water cases at the bottom part of the core sample. This phenomenon implies that the steam-water capillary pressures are equal to the air-water capillary pressures at the bottom part of the core, which is also observed in the imbibition case (see Figure 3).

The reason that the drainage capillary pressure curves were not calculated was because the water saturations could not

be determined easily due to the X-ray beam hardening effect. But we did observe the similar trend of the difference between steam-water and air-water capillary pressures in drainage by comparing the CT numbers in the core in both steam-water and air-water cases.

4.1.3 A Phenomenological Model for Explaining the Differences between Steam-Water and Air-Water Flow

Experimentally we have found that the differences between steam-water and air-water capillary pressures as well as relative permeability (Horne *et al.*, 2000; Chen *et al.*, 2003 and 2004) are significant. However there have been no theoretical models to explain why there are differences. To this end, we developed such a phenomenological model, as shown in Figure 5.

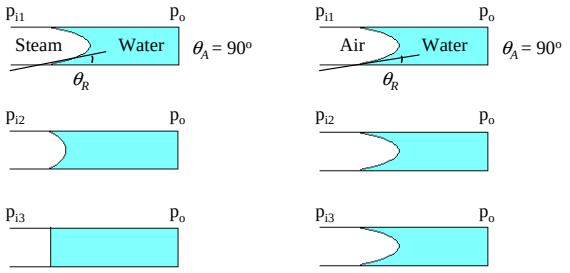

(a) Steam-Water (b) Air-Water

Figure 5: A Phenomenological model for explaining the differences between steam-water and air-water flow.

Let us consider a simple situation: steam-water and air-water flows in a single capillary tube with a constant temperature. Figure 5a shows the steam-water flow and Figure 5b shows the air-water flow. The potential flow direction is assumed to be from left to right. For simplicity, the advancing contact angle (θ_A) at the outlet is assumed to be 90^o. The outlet pressure is constant and is equal to p_o. The inlet pressure changes from p_{i1} to p_{i3}. p_{ij} (j=1, 2, 3) is greater than p_o. Also assumed is that p_{i1} is close to the saturation pressure and the differential pressure (p_{i1} - p_o) is less than the capillary pressure, P_{c1}, corresponding to the receding contact angle θ_R. In this case, neither steam-water nor air-water interfaces can move through the single capillary tube. When the inlet pressure increases to p_{i2} and approaches the saturation pressure, steam may condense to liquid water if the differential pressure (p_{i2} - p_o) is less than the capillary pressure, P_{c2}. One outcome resulting from the condensation may be the increase in the receding contact angle. This will reduce the steam-water capillary pressure. When the inlet pressure further increases to p_{i3} with a value greater than the saturation pressure (but p_{i3} - p_o still less than P_{c1}), the receding contact angle may be equal to 90^{o}and the steam-water capillary pressure (P_{c3}) may be equal to zero. In this case, steam and water can flow through the tube. However air-water capillary pressure stays constant so air and water cannot flow through the tube as the inlet pressure increases from p_{i1} to p_{i3}.

Based on this phenomenological model, steam-water capillary pressure may be smaller than air-water capillary pressure because of the condensation. Therefore the resistance to steam-water flow may also be smaller than to air-water flow. According to the discussion by Li and Horne (2004a), steam-water relative permeability is greater than air-water relative permeability if steam-water capillary pressure is smaller than air-water capillary pressure, as reported by Horne *et al.* (2000) and Chen *et al.* (2004).

4.2 Steam-Water Capillary Pressures Measured Using a Steady-State Flow Method

As mentioned previously, we may not be able to substitute for steam-water capillary pressures simply by using air-water capillary pressure measurements. Therefore it may be necessary to measure steam-water capillary pressures directly. The results of direct measurements using a steady-state flow approach are discussed in this section.

Both the drainage and imbibition steam-water capillary pressures calculated using Eqs. 1 and 2 with the experimental data (Mahiya, 1999) are shown in Figure 6. During the experimental process, the water saturation was first decreased from 100% to the remaining water saturation, about 28%, representing a drainage process. The water saturation was then increased, representing an imbibition. The entry capillary pressure of steam is small for this sample. The drainage steam-water capillary pressure in the sample at a water saturation of about 30% is around 0.613 atm, as shown in Figure 6. The water saturation remaining in the core sample after the drainage by steam flooding was about 28%. The actual residual water saturation may be slightly less than this value because of practical limitations on the duration of the experiments; it may be estimated using a regression analysis with the experimental data.

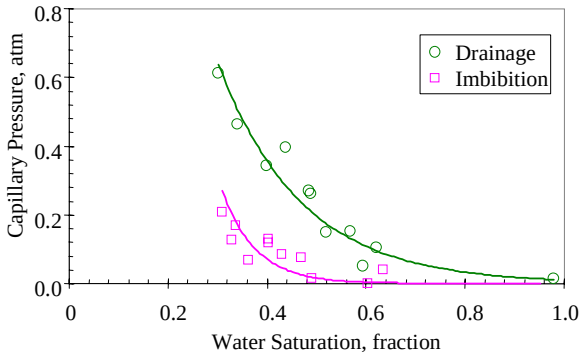

Figure 6: Steam-water capillary pressure curves in high permeability sandstone.

Also shown in Figure 6 is the imbibition curve. The imbibition steam-water capillary pressure at a water saturation of about 30% is around 0.206 atm which is much less than the drainage steam-water capillary pressure at the same water saturation. The imbibition values are actually less than the drainage values over the whole range of water saturation (see Figure 6). This observation is consistent with that in gas-liquid systems. As an example, Leverett (1941) found that the imbibition air-water capillary pressure was less than the drainage capillary pressure in a sand pack.

4.3 A Steam-Water Capillary Pressure Model Based on Experimental Data

Capillary pressure data are often required for numerical simulations and other reservoir engineering calculations. It would be useful for reservoir engineers to have an approach to estimate the values of steam-water capillary pressure for geothermal rocks with any porosity and permeability at any reservoir temperature. Until now, geothermal reservoir engineers have usually guessed at the form of the steam-water capillary pressure curve used for numerical simulation, or ignored it entirely.

Both drainage and imbibition steam-water capillary pressure models were developed by Li and Horne (2002a) based on experimental data for application in geothermal

reservoir engineering. The models are presented and discussed here.

4.3.1 Drainage Case

The drainage steam-water capillary pressure model proposed by Li and Horne (2002a) is expressed as follows:

$$P_c = 40.12 \frac{\sigma}{\sqrt{\frac{k}{\phi}}} (S^*_{wd})^{-1.843} \quad (6)$$

where the units of P_c, σ and k are atm, dynes/cm, and nd respectively; ϕ and S^*_{wd} are expressed as fractions. The porosity and permeability of reservoir rocks would need to be measured. The surface tension can be calculated once the reservoir temperature is known. Therefore the steam-water capillary pressure curve for geothermal reservoir rocks may be obtained using Eq. 6. The model expressed in Eq. 6 is suitable for drainage processes and is based on the assumptions: (1) contact angle does not change with permeability and temperature; (2) rock samples have the same *J*-functions (Li and Horne, 2002a).

$$S^*_{wd} = \frac{S_w - S_{wr}}{1 - S_{wr}} \quad (7)$$

where S_{wr} and S^*_{wd} are the residual water saturation and normalized water saturation.

Figure 7 shows theoretical data of steam-water capillary pressures calculated using the model (Eq. 6) for rock samples with permeability ranging from 1.3 to 500 nd (a typical range of permeability in The Geysers rock). The porosity used in the calculation was 1.9%. The surface tension at a temperature of 240°C is 28.41mN/m.

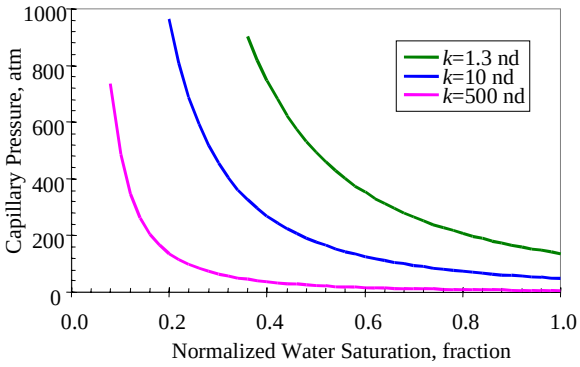

Figure 7: Drainage steam-water capillary pressure curves at 240°C for rock with different permeability (Powell and Li, 2003).

Note that this model (Eq. 6) was derived based on the assumption that the capillary pressure curves of geothermal rock could be represented mathematically using the Brooks-Corey model (1964). The Brooks-Corey model is expressed as follows:

$$P_c = p_e (S^*_{wd})^{-1/\lambda} \quad (8)$$

where p_e is the entry capillary pressure and λ is the pore size distribution index.

We found later that some rock samples, such as those from The Geysers geothermal field, may not be represented using the Brooks-Corey model (Li and Horne, 2003a; Li, 2004a). In this case, one may need to use a different model. We will discuss this in more detail later.

4.3.2 Imbibition Case

For the imbibition steam-water capillary pressure curve, Li and Horne (2001) proposed a model:

$$P_c = p_m (1 - S^*_{wimb})^d \quad (9)$$

here p_m is the capillary pressure at S_{wi}; d is a fitting coefficient for the imbibition capillary pressure function. S^*_{wimb} is the normalized water saturation which is defined as follows:

$$S^*_{wimb} = \frac{S_w - S_{wi}}{1 - S_{wi} - S_{sr}} \quad (10)$$

where S_{wi} is the initial water saturation for imbibition; it is equal to the residual water saturation by drainage. S_{sr} is the residual steam saturation by imbibition.

Assuming that the capillary pressure follows this model (Eq. 9), we proposed an approach to calculate imbibition steam-water capillary pressure based on experimental data (Li and Horne, 2002a). The model is expressed as follows:

$$P_c = 888.6 \frac{\sigma}{\sqrt{\frac{k}{\phi}}} (1 - S^*_{wimb})^{5.539} \quad (11)$$

where the units of P_c, σ and k are atm, dynes/cm, and nd respectively; ϕ and S^*_{wimb} are expressed as fractions. The surface tension can be calculated once the reservoir temperature is known. The model expressed in Equation 11 is suitable for imbibition processes (for example, water injection process) in which water saturation increases and is based on the same assumptions as the drainage model.

Example data of steam-water capillary pressure in the imbibition case were calculated using the imbibition model (Eq. 11) for rock samples with permeability ranging from 1.3 to 500 nd. The results are plotted in Figure 8. The porosity, surface tension, and the temperature are the same as those used in Figure 7.

One feature of the steam-water capillary pressure models for both drainage (Eq. 6) and imbibition (Eq. 11) is that these models are developed based on experimental data. On the other hand, these models are simple. The only required parameters are reservoir temperature, pressure, porosity and permeability.

Although they are simple, these models would be useful and helpful for reservoir engineers to reduce the uncertainty in numerical simulation or other calculations. Therefore, engineering and financial risks would be reduced.

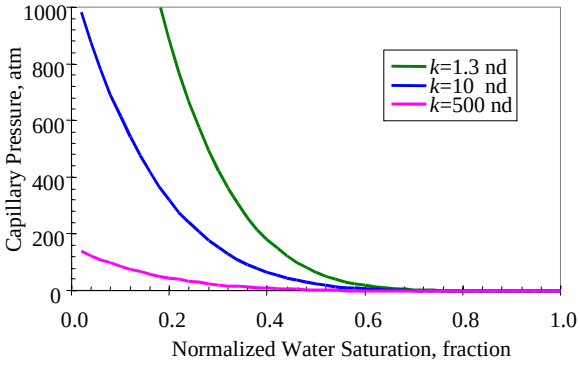

Figure 8: Imbibition steam-water capillary pressure curves at 240°C for rock with different permeability.

As mentioned previously, imbibition capillary pressure is usually less than drainage capillary pressure. This can also be seen by comparing Figure 7 to Figure 8.

4.4 A Generalized Capillary Pressure Model Based on Fractal Modeling of a Porous Medium

Recently Li and Horne (2003a) found that the frequently used Brooks-Corey model could not be used to represent the capillary pressure data measured in The Geysers rock samples using a mercury intrusion technique. In fact, few existing capillary pressure models work for these rock samples.

Interestingly, Li and Horne (2003a) found that fractal curves inferred from capillary pressure data were good straight lines for both Berea sandstone in which the Brooks-Corey model works and The Geysers rock samples in which the Brooks-Corey model does not work. This finding implies that a more general capillary pressure model may exist to represent both of the rocks. Such a model has been developed (Li, 2004b; Li and Horne, 2004b) and is expressed as follows:

$$P_c = p_{\max}(1 - bS_w^*)^{-\frac{1}{\lambda}} \qquad (12)$$

where $p_{\max}$ is the capillary pressure at the residual nonwetting phase saturation in the imbibition case or the capillary pressure at the residual wetting phase saturation in the drainage case. S_w^* is the normalized saturation of the wetting phase. b is a constant associated with pore size (represented by p_e and p_{max}) and its distribution (represented by λ); b is expressed as follows:

$$b = 1 - \left(\frac{p_e}{p_{\max}}\right)^{-\lambda} \qquad (13)$$

where λ = 3 - D_f. D_f is the fractal dimension, which is a representation of the heterogeneity of rock. The greater the fractal dimension, the greater the heterogeneity. Note that the pore size distribution index λ in the Brooks-Corey capillary pressure model is also a representation of the heterogeneity. The greater the pore size distribution index, the less the heterogeneity of the porous medium.

For D_f<3, if p_{max} approaches infinity, then the generalized capillary pressure model (Eq. 12) can be reduced to the Brooks-Corey model (Eq. 8). Note that S_w^* is equal to S_{wd}^* in this case.

In the case in which b=1, the generalized capillary pressure model (Eq. 12) can be reduced to the Li and Horne model (Eq. 9).

The reductions described previously demonstrate that the Brooks-Corey model for the drainage case and the Li-Horne model for the imbibition case may have a solid theoretical basis.

When b=0, the generalized capillary pressure model (Eq. 12) can then be reduced to: $P_c = p_{\max}$. This may be considered a capillary pressure model for a single capillary tube.

One can see that Eq. 12, as a generalized capillary pressure model, could be applied in both a complicated porous medium and in a single capillary tube as well as in both drainage and imbibition cases.

Figure 9 shows theoretical capillary pressure data calculated using the generalized model (Eq. 12) with different values of fractal dimension. The values of maximum capillary pressure and entry capillary pressure were 100 atm and 0.4 atm respectively in Figure 9. The residual wetting-phase saturation was 20%.

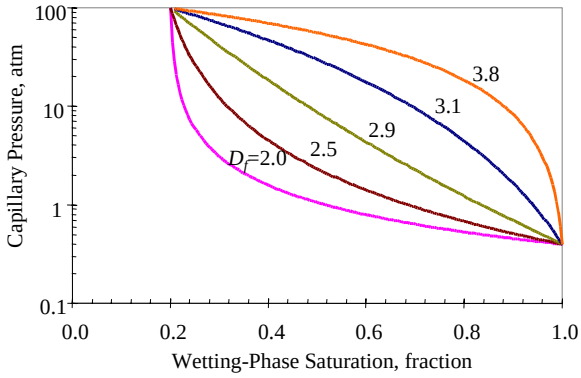

Figure 9: Typical capillary pressure curves calculated using the new model with different values of fractal dimension.

In the case where D_f<3.0, the capillary pressure curve is convex to the axis of the wetting-phase saturation and looks like a common capillary pressure curve (for example, the capillary pressure curve of Berea sandstone). This type of capillary pressure curve can usually be represented mathematically by the Brooks-Corey model in cases in which p_e/p_{max} is negligible. In the case where D_f>3.0, the capillary pressure curve is concave to the axis of the wetting-phase saturation (see Figure 9). The capillary pressure curves of The Geysers rock have such a feature (Li and Horne, 2003a).

4.5 Verification and Application of a Generalized Capillary Pressure Model

As mentioned previously, the frequently used Brooks-Corey model could not represent the capillary pressure behavior of The Geysers rock samples. A typical capillary pressure curve of The Geysers rock is shown in Figure 10. The capillary pressures were measured using a mercury intrusion technique. It is obvious that the Brooks-Corey model cannot represent such a curve. The new capillary pressure model (Eq. 12) was used to match the data and the results are demonstrated in Figure 10. One can see that the generalized capillary pressure model can represent the data of The Geysers rock satisfactorily. The values of

parameters obtained by the match were: p_{max}=1.837×10^3 atm, b=0.984, and D_f =3.483.

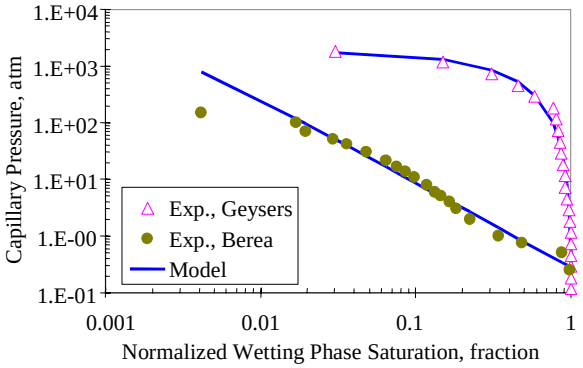

Figure 10: Fit to the normalized capillary pressure curves of Berea sandstone and The Geysers rock.

The capillary pressure data of Berea sandstone, measured using a mercury intrusion technique, were also modeled using the new model and the results are plotted in Figure 10. One can see that the generalized model can also fit the capillary pressures of Berea sandstone appropriately. The values of parameters obtained by the match were: p_{max}=1.0×10^4 atm, p_e =0.28 atm, and D_f =2.33. The Brooks-Corey model can be applied directly if the normalized capillary pressure curve is linear on a log-log plot. This is because the generalized capillary pressure model (Eq. 12) can be reduced to the Brooks-Corey model in this case.

Figure 10 shows that the generalized model can represent the capillary pressure curves of both Berea sandstone and The Geysers rock.

More examples verifying the new capillary pressure model (Eq. 12) were reported recently in another paper (Li and Horne, 2004b).

4.6 Computation of Relative Permeability from Experimental Data of Capillary Pressure

Li and Horne (2004a) found significant differences between steam-water and air-water capillary pressures, and Horne *et al.* (2000) found differences between steam-water and air-water relative permeabilities. According to these studies, steam-water flow properties may not be replaced simply by air-water or nitrogen-water flow properties. On the other hand, it is very difficult to measure steam-water relative permeability. It would be helpful for reservoir engineers to be able to calculate steam-water relative permeability once steam-water capillary pressure data are available.

There are two main approaches to infer relative permeability from capillary pressure data. One is the Purcell approach (1949) and the other is the Burdine approach (1953).

4.6.1 Based on the Purcell Approach

Purcell (1949) developed an equation to compute rock permeability by using capillary pressure data. This equation can be extended readily to the calculation of multiphase relative permeability. In two-phase flow, the relative permeability of the wetting phase can be calculated as follows:

$$k_{rw} = \frac{\int_0^{S_w} dS_w/(P_c)^2}{\int_0^1 dS_w/(P_c)^2} \qquad (14)$$

where k_{rw} and S_w are the relative permeability and saturation of the wetting phase (the water phase in steam-water flow).

Similarly, the relative permeability of the nonwetting phase (the steam phase in steam-water flow) can be calculated as follows:

$$k_{rnw} = \frac{\int_{S_w}^1 dS_w/(P_c)^2}{\int_0^1 dS_w/(P_c)^2} \qquad (15)$$

where k_{rnw} is the relative permeability of the nonwetting phase. It can be seen from Eqs. 14 and 15 that the sum of the wetting and nonwetting phase relative permeabilities at a specific saturation is equal to one. This may not be true in most porous media.

Substituting the generalized capillary pressure model (Eq. 12) into Eqs. 14 and 15:

$$k_{rw} = \frac{1-(1-bS_w^*)^m}{1-(1-b)^m} \qquad (16)$$

$$k_{rnw} = \frac{(1-bS_w^*)^m-(1-b)^m}{1-(1-b)^m} \qquad (17)$$

where m is expressed as follows:

$$m = \frac{2+\lambda}{\lambda} = \frac{5-D_f}{3-D_f} \qquad (18)$$

When D_f<3 and $p_{\max}$ approaches infinity, Eqs. 16 and 17 can be reduced to the simple Purcell relative permeability model expressed as follows:

$$k_{rw} = (S_w^*)^{\frac{2+\lambda}{\lambda}} \qquad (19)$$

$$k_{rnw} = 1-(S_w^*)^{\frac{2+\lambda}{\lambda}} \qquad (20)$$

Therefore the generalized relative permeability model (Eqs. 16 and 17) encompasses the Purcell relative permeability model (Eqs. 19 and 20).

4.6.2 Based on the Burdine Approach

The relative permeability model derived from the generalized capillary pressure model using the Burdine approach is expressed as follows:

$$k_{rw} = \frac{(S_w^*)^2[1-(1-bS_w^*)^m]}{1-(1-b)^m} \qquad (21)$$

$$k_{rnw} = \frac{(1-S_w^*)^2[(1-bS_w^*)^m-(1-b)^m]}{1-(1-b)^m} \qquad (22)$$

The difference from the Purcell approach is that a tortuosity factor as a function of the wetting phase saturation is introduced in the Burdine approach. Detailed derivation of Eqs. 21 and 22 is reported by Li (2004b).

In the case in which D_f<3 and $p_{\max}$ approaches infinity, Eqs. 21 and 22 can be reduced to the simple Brooks-Corey relative permeability model, which is expressed as follows:

$$k_{rw} = (S_w^*)^{\frac{2+3\lambda}{\lambda}} \quad (23)$$

$$k_{rnw} = (1-S_w^*)^2[1-(S_w^*)^{\frac{2+\lambda}{\lambda}}] \quad (24)$$

Figure 11 shows a set of typical relative permeability curves calculated using the generalized model (Eqs. 16 and 22).

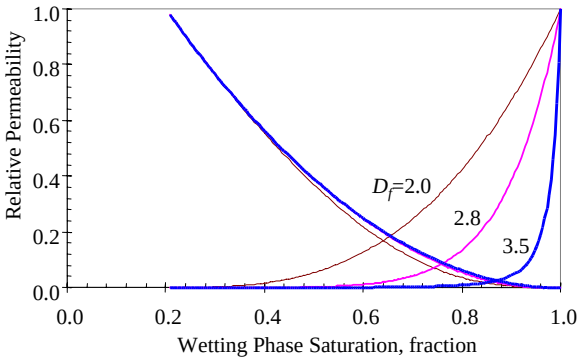

Figure 11: Typical relative permeability curves calculated using the new model with different values of fractal dimension.

The wetting phase relative permeability was calculated using Eq. 16 and the nonwetting phase relative permeability was calculated using Eq. 22 with different values of fractal dimension. The reason to do this was because Li and Horne (2002b) reported that the Purcell model is the best fit to the experimental data of the wetting phase relative permeability for both drainage and imbibition processes. However the Purcell model does not work for the nonwetting phase while the Burdine approach does.

One can see that the relative permeability of the nonwetting phase does not change much with fractal dimension. On the other hand, the relative permeability of the wetting phase increases with the decrease in fractal dimension.

Figure 11 also shows that the wetting phase relative permeability curves with fractal dimension greater than 3.0 have different features from those with fractal dimension less than 3.0, as predicted by the model (see Eq. 16). As an example, Berea sandstone usually has a fractal dimension less than 3.0 (Li, 2004b) and The Geysers rock usually has a fractal dimension greater than 3.0. One can see that the values of the wetting phase relative permeability in the case where the fractal dimension is over 3.0 are very small until the wetting phase saturation reaches about 80%. This phenomenon may be verified by future experimental data of relative permeability measured in The Geysers rock.

4.6.3 Experimental Verification of the Calculation of Relative Permeability from Capillary Pressure

Experimental data of relative permeability in rock with a fractal dimension greater than 3.0 (such as The Geysers rock) are not available at present. Therefore we discuss only the case with a fractal dimension smaller than 3.0. Such an example rock is Berea sandstone.

The drainage steam-water relative permeabilities were calculated using the Purcell and other models with the experimental data of the drainage steam-water capillary pressure shown in Figure 6. The calculated results and the comparison to the corresponding experimental data are shown in Figure 12. The relative permeabilities in Figure 12 were normalized to conduct the comparison. The method to do this is to divide the experimental relative permeability by the corresponding end-point value. More details on this calculation are reported by Li and Horne (2002b).

We can see from Figure 12 that the water relative permeabilities calculated using the Purcell model (Eq. 19) are the best fit to the experimental data. This implies that it may not be necessary to adjust the calculation of the wetting phase relative permeabilities by introducing the concept of the tortuosity factor in such a case. The water phase relative permeabilities calculated by all the other models are less than the experimental values. It can be seen from Figure 12 that the steam phase (nonwetting phase) relative permeabilities calculated by all the models except the Purcell model are almost the same and consistent with the experimental data in the drainage case. The steam phase relative permeabilities calculated by the Purcell model are not shown in Figure 12 because the curve is concave downwards, which is unexpected and far from the experimental values.

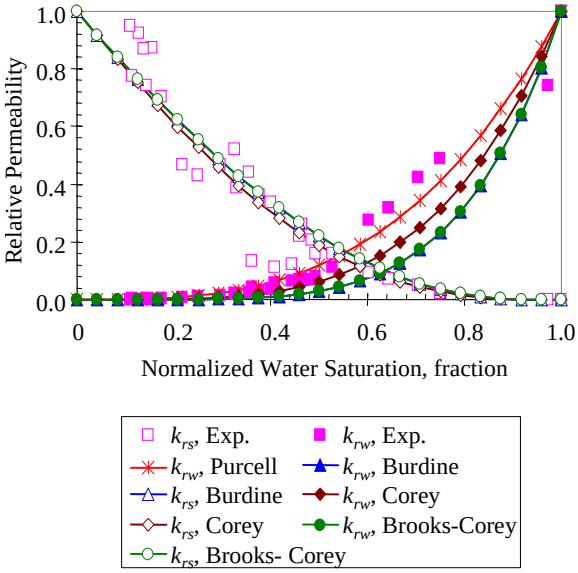

Figure 12: Calculated steam-water relative permeability and the comparison to the experimental data from Mahiya[16] in drainage.

Li and Horne (2002b) reported more examples to verify the use of the Purcell model (Eq. 19) to calculate the wetting phase relative permeability and the Brooks-Corey model (Eq. 24) to calculate the nonwetting phase relative permeability.

Figure 12 also demonstrates that steam-water relative permeabilities can be calculated from steam-water capillary pressure. As pointed out by Li and Horne (2003b), there are many advantages in doing so. These advantages are described briefly here. Measurements of steam-water relative permeabilities over the full range of water saturation are usually time-consuming, expensive, and inaccurate in many cases. On the other hand, uncertainty may be reduced because the number of input parameters to numerical simulators is reduced. Reservoir engineering computations may be more efficient, more economical, more consistent, and more reliable by using the capillary pressure methods to obtain relative permeabilities.

5. CONCLUSIONS

1. Based on experimental data, steam-water capillary pressures are less than air-water capillary pressure. Steam-water values may not be substituted simply using air-water values.

2. A phenomenological model has been proposed to explain the differences between steam-water and air-water flow.

3. A formula has been derived on the basis of the Kelvin equation to calculate steam-water capillary pressure using experimental data of temperature and pressure from the steady-state flow of steam and water in porous media.

4. An empirical model has been developed to calculate steam-water capillary pressure directly using a very limited number of reservoir parameters. These parameters include porosity, permeability, and temperature.

5. A generalized theoretical model has been developed to represent capillary pressure curves or pore size distribution of a porous medium and has been verified experimentally. The generalized model can be reduced to the Brooks-Corey model for the drainage case and the Li-Horne model for the imbibition case.

6. Relative permeability can be calculated from capillary pressure based on the generalized relative permeability model, which is inferred from the generalized capillary pressure model. When fractal dimension is less than 3, the Purcell model is proposed to calculate the water relative permeability and the Brooks-Corey model to calculate the steam relative permeability.

ACKNOWLEDGMENTS

This research was conducted with financial support to the Stanford Geothermal Program from the US Department of Energy under grant DE-FG07-02ID14418, the contribution of which is gratefully acknowledged. The assistance of Huda Nassori and Will Whitted in constructing and installing the apparatus is gratefully acknowledged.

REFERENCES

Ambusso, W.J.: “Experimental Determination of Steam-Water Relative Permeability Relations,” MS thesis, Stanford University, Stanford, CA, USA (1996).

Brooks, R.H. and Corey, A.T.: “Hydraulic Properties of Porous Media,” Colorado State University, Hydro paper No. 5 (1964).

Burdine, N. T.: "Relative Permeability Calculations from Pore Size Distribution Data," Trans. *AIME*, (1953), **198**, 71.

Chen, C.Y., Li, K., and Horne, R.N.: “Difference Between Steam-Water and Air-Water Relative Permeabilities in Fractures,” Proceedings of the GRC 2003 annual meeting, October 12-15, 2003, Morelia, Mexico; *GRC* Trans. V. **27** (2003).

Chen, C.Y., Li, K., and Horne, R.N.: “Experimental Study of Phase Transformation Effects on Relative Permeabilities in a Fracture,” SPE 90233, Proceedings of the 2004 SPE Annual Technical Conference and Exhibition, Houston, Texas, U.S.A., 27–29 September 2004.

Horne, R.N., Satik, C., Mahiya, G., Li, K., Ambusso, W., Tovar, R., Wang, C., and Nassori, H.: “Steam-Water Relative Permeability,” Proceedings of the World Geothermal Congress 2000, Kyushu-Tohoku, Japan, May 28-June 10, 2000, p. 2609-2615.

Horne, R.N., Ramey, H.J. Jr., Shang, S., Correa, A., and Hornbrook, J.: “The Effects of Adsorption and Desorption on Production and Reinjection in Vapor-Dominated Geothermal fields,” Proceedings of the World Geothermal Congress 1995, Florence, Italy, May 1995, 1973-1977.

Leverett, M.C.: “Capillary Behavior in Porous Solids,” *Trans*., AIME, (1941), **142**, 152-168.

Li, K. and Horne, R.N.: “An Experimental and Theoretical Study of Steam-Water Capillary Pressure,” *SPEREE* (December 2001), p. 477-482.

Li, K. and Horne, R.N. (2002a): “A Capillary Pressure Model for Geothermal Reservoirs,” Proceedings of the GRC 2002 annual meeting, September 23-25, 2002, Reno, USA; *GRC* Trans. V. **26** (2002).

Li, K. and Horne, R.N. (2002b): “Experimental Verification of Methods to Calculate Relative Permeability Using Capillary Pressure Data,” SPE 76757, Proceedings of the 2002 SPE Western Region Meeting/AAPG Pacific Section Joint Meeting held in Anchorage, Alaska, May 20-22, 2002.

Li, K. and Horne, R.N. (2003a): “Fractal Characterization of The Geysers Rock,” Proceedings of the GRC 2003 annual meeting, October 12-15, 2003, Morelia, Mexico; *GRC* Trans. V. **27**.

Li, K. and Horne, R.N. (2003b): “Numerical Simulation with Input Consistency between Capillary Pressure and Relative Permeability,” SPE 79716, Proceedings of the 2003 SPE Reservoir Simulation Symposium held in Houston, Texas, U.S.A., 3–5 February 2003.

Li, K. and Horne, R.N. (2004a): “Steam-Water and Air-Water Capillary Pressures: Measurement and Comparison,” *J. of Canadian Petroleum Technology* (July 2004), V.43, No. 7.

Li, K. and Horne, R.N. (2004b): “A Universal Capillary Pressure Model: Verification and Application,” Proceedings of the GRC 2004 annual meeting, Palm Springs, California, U.S.A., August 29 - September 1, 2004.

Li, K. (2004a): “Characterization of Rock Heterogeneity Using Fractal Geometry,” SPE 86975, Proceedings of the 2004 SPE Western Region Meeting, Bakersfield, CA, USA, March 16-18, 2004.

Li, K. (2004b): “Generalized Capillary Pressure and Relative Permeability Model Inferred From Fractal Characterization of Porous Media,” SPE 89874, Proceedings of the 2004 SPE Annual Technical Conference and Exhibition, Houston, Texas, U.S.A., 27–29 September 2004.

Mahiya, G.F.: Experimental Measurement of Steam-Water Relative Permeability, MS thesis, Stanford University, Stanford, CA, USA, 1999.

Purcell, W.R.: "Capillary Pressures-Their Measurement Using Mercury and the Calculation of Permeability", Trans. *AIME*, (1949), **186**, 39.

Persoff, P. and Hulen, J.B.: “Hydrologic Characterization of Four Cores from the Geysers Coring Project,”

Proceedings of 21st Workshop on Geothermal Reservoir Engineering, Stanford, CA, USA, 1996, p. 327-334.

Powell, T. and Li, K.: "A Depletion Mechanism for the Behavior of Noncondensible Gases at The Geysers," Proceedings of the GRC 2003 annual meeting, October 12-15, 2003, Morelia, Mexico; *GRC* Trans. V. **27** (2003).

Sanchez, J.M. and Schechter, R.S.: "Comparison of Two-Phase Flow of Steam/Water through an Unconsolidated Permeable Medium, " *SPERE*, (Aug. 1990), p. 293-300.

Satik, C.: "A Measurement of Steam-Water Relative Permeability," Proceedings of 23rd Workshop on Geothermal Reservoir Engineering, Stanford University, Stanford, CA, USA, 1998, p. 120-126.

Sta. Maria, R.B. and Pingol, A.S.: "Simulating the Effects of Adsorption and Capillary Forces in Geothermal Reservoirs," Proceedings of 21st Workshop on Geothermal Reservoir Engineering, Stanford, CA, USA, 1996, p. 165-173.

Tsypkin, G.G. and Calore, C.: "Capillary Pressure Influence on Water Vaporization in Geothermal Reservoirs," Proceedings of 24th Workshop on Geothermal Reservoir Engineering, Stanford, CA, USA, 1999, p. 359-367.

Urmeneta, N.A., Fitzgerald, S., and Horne, R.N.: "The Role of Capillary Forces in the Natural State of Fractured Geothermal Reservoirs," Proceedings of 23rd Workshop on Geothermal Reservoir Engineering, Stanford, CA, USA, 1998, p. 100-109.